

MIT Open Access Articles

The mTORC1 Pathway Stimulates Glutamine Metabolism and Cell Proliferation by Repressing SIRT4

The MIT Faculty has made this article openly available. **Please share** how this access benefits you. Your story matters.

Citation: Csibi, Alfred, Sarah-Maria Fendt, Chenggang Li, George Pouligiannis, Andrew Y. Choo, Douglas J. Chapski, Seung Min Jeong, et al. "The mTORC1 Pathway Stimulates Glutamine Metabolism and Cell Proliferation by Repressing SIRT4." *Cell* 153, no. 4 (May 2013): 840–854. © 2013 Elsevier Inc.

As Published: <http://dx.doi.org/10.1016/j.cell.2013.04.023>

Publisher: Elsevier

Persistent URL: <http://hdl.handle.net/1721.1/91506>

Version: Final published version: final published article, as it appeared in a journal, conference proceedings, or other formally published context

Terms of Use: Article is made available in accordance with the publisher's policy and may be subject to US copyright law. Please refer to the publisher's site for terms of use.



The mTORC1 Pathway Stimulates Glutamine Metabolism and Cell Proliferation by Repressing SIRT4

Alfred Csibi,¹ Sarah-Maria Fendt,^{2,6} Chenggang Li,^{3,5} George Poulgiannis,^{4,5} Andrew Y. Choo,¹ Douglas J. Chapski,¹ Seung Min Jeong,¹ Jamie M. Dempsey,¹ Andrey Parkhitko,³ Tasha Morrison,³ Elizabeth P. Henske,³ Marcia C. Haigis,¹ Lewis C. Cantley,⁴ Gregory Stephanopoulos,² Jane Yu,³ and John Blenis^{1,*}

¹Department of Cell Biology, Harvard Medical School, Boston, MA 02115, USA

²Department of Chemical Engineering, Massachusetts Institute of Technology, Cambridge, MA 02139, USA

³Division of Pulmonary and Critical Care Medicine, Department of Medicine, Brigham and Women's Hospital, Boston, MA 02115, USA

⁴Division of Signal Transduction, Beth Israel Medical Center and Department of Systems Biology, Harvard Medical School, Boston, MA 02115, USA

⁵These authors contributed equally to this work

⁶Present address: Vesalius Research Center, Flemish Institute of Biotechnology (VIB), B 3000 Leuven, Belgium

*Correspondence: john_blenis@hms.harvard.edu

<http://dx.doi.org/10.1016/j.cell.2013.04.023>

SUMMARY

Proliferating mammalian cells use glutamine as a source of nitrogen and as a key anaplerotic source to provide metabolites to the tricarboxylic acid cycle (TCA) for biosynthesis. Recently, mammalian target of rapamycin complex 1 (mTORC1) activation has been correlated with increased nutrient uptake and metabolism, but no molecular connection to glutaminolysis has been reported. Here, we show that mTORC1 promotes glutamine anaplerosis by activating glutamate dehydrogenase (GDH). This regulation requires transcriptional repression of *SIRT4*, the mitochondrial-localized sirtuin that inhibits GDH. Mechanistically, mTORC1 represses *SIRT4* by promoting the proteasome-mediated destabilization of cAMP-responsive element binding 2 (CREB2). Thus, a relationship between mTORC1, *SIRT4*, and cancer is suggested by our findings. Indeed, *SIRT4* expression is reduced in human cancer, and its overexpression reduces cell proliferation, transformation, and tumor development. Finally, our data indicate that targeting nutrient metabolism in energy-addicted cancers with high mTORC1 signaling may be an effective therapeutic approach.

INTRODUCTION

Nutrient availability plays a pivotal role in the decision of a cell to commit to cell proliferation. In conditions of sufficient nutrient sources and growth factors (GFs), the cell generates enough energy and acquires or synthesizes essential building blocks at a sufficient rate to meet the demands of proliferation.

Conversely, when nutrients are scarce, the cell responds by halting the biosynthetic machinery and by stimulating catabolic processes such as fatty-acid oxidation and autophagy to provide energy maintenance (Vander Heiden et al., 2009). Essential to the decision process between anabolism and catabolism is the highly conserved, atypical serine/threonine kinase mammalian target of rapamycin complex 1 (mTORC1), whose activity is deregulated in many cancers (Menon and Manning, 2008). This complex, which consists of mTOR, Raptor, and mLST8, is activated by amino acids (aa), GFs (insulin/IGF-1), and cellular energy to drive nutrient uptake and subsequently proliferation (Yecies and Manning, 2011). The molecular details of these nutrient-sensing processes are not yet fully elucidated, but it has been shown that aa activate the Rag guanosine-5'-triphosphate (GTP)ases to regulate mTORC1 localization to the lysosomes (Kim et al., 2008; Sancak et al., 2008), and GFs signal through the PI3K-Akt or the extracellular signal-regulated kinase (ERK)-ribosomal protein S6 kinase (RSK) pathways to activate mTORC1 by releasing the Ras homolog enriched in brain (RHEB) GTPase from repression by the tumor suppressors tuberous sclerosis 1 (TSC1)-TSC2 (Inoki et al., 2002; Manning et al., 2002; Roux et al., 2004). Finally, low-energy conditions inhibit mTORC1 by activating AMPK and by repressing the assembly of the TTT-RUVBL1/2 complex (Inoki et al., 2003; Gwinn et al., 2008; Kim et al., 2013).

Glutamine, the most abundant aa in the body, plays an important role in cellular proliferation. It is catabolized to α -ketoglutarate (α KG), an intermediate of the tricarboxylic acid (TCA) cycle, through two deamination reactions in a process termed glutamine anaplerosis (DeBerardinis et al., 2008). The first reaction requires glutaminase (GLS) to generate glutamate, and the second occurs by the action of either glutamate dehydrogenase (GDH) or transaminases. Incorporation of α KG into the TCA cycle is the major anaplerotic step critical for the production of biomass building blocks including nucleotides, lipids, and aa (Wise and Thompson, 2010). Recent studies have demonstrated

that glutamine is also an important signaling molecule. Accordingly, it positively regulates the mTORC1 pathway by facilitating the uptake of leucine (Nicklin et al., 2009) and by promoting mTORC1 assembly and lysosomal localization (Durán et al., 2012; Kim et al., 2013).

Commonly occurring oncogenic signals directly stimulate nutrient metabolism, resulting in nutrient addiction. Oncogenic levels of Myc have been linked to increased glutamine uptake and metabolism through a coordinated transcriptional program (Wise et al., 2008; Gao et al., 2009). Hence, it is not surprising that cancer cells are addicted to glutamine (Wise and Thompson, 2010). Thus, considering the prevalence of mTORC1 activation in cancer and the requirement of nutrients for cell proliferation, understanding how mTORC1 activation regulates nutrient levels and metabolism is critical. Activation of the mTORC1 pathway promotes the utilization of glucose, another nutrient absolutely required for cell growth. However, no study has yet investigated if and how the mTORC1 pathway regulates glutamine uptake and metabolism. Here, we describe a role of the mTORC1 pathway in the stimulation of glutamine anaplerosis by promoting the activity of GDH. Mechanistically, mTORC1 represses the transcription of *SIRT4*, an inhibitor of GDH. *SIRT4* is a mitochondrial-localized member of the sirtuin family of nicotinamide adenine dinucleotide (NAD)-dependent enzymes known to play key roles in metabolism, stress response, and longevity (Haigis and Guarente, 2006). We demonstrate that the mTORC1 pathway negatively controls *SIRT4* by promoting the proteasome-mediated degradation of cAMP-responsive element-binding (CREB) 2. We reveal that *SIRT4* levels are decreased in a variety of cancers, and when expressed, *SIRT4* delays tumor development in a *Tsc2*^{-/-} mouse embryonic fibroblast (MEF) xenograft model. Thus, our findings provide insights into how mTORC1 regulates glutamine anaplerosis, contributing therefore to the metabolic reprogramming of cancer cells, an essential hallmark to support their excessive need for proliferation.

RESULTS

The mTORC1 Pathway Regulates Glutamine Metabolism via GDH

The activation of the mTORC1 pathway has recently been linked to glutamine addiction of cancer cells (Choo et al., 2010), yet it remains to be resolved whether mTORC1 serves as a regulator of glutamine anaplerosis. To investigate this possibility, we first determined the effect of mTORC1 activity on glutamine uptake. We measured glutamine uptake rates in *Tsc2* wild-type (WT) and *Tsc2*^{-/-} MEFs. We found that *Tsc2*^{-/-} MEFs consumed significantly more glutamine (Figure 1A), showing that mTORC1 activation stimulates the uptake of this nutrient. In addition, re-expression of *Tsc2* in *Tsc2*^{-/-} cells reduced glutamine uptake (Figure S1A available online). Similarly, mTORC1 inhibition with rapamycin resulted in decreased glutamine uptake in MEFs (Figure 1A). The decrease in glutamine uptake was significantly reduced after 6 hr of rapamycin treatment when compared to control (data not shown). To further confirm the role of mTORC1 on glutamine uptake, we used human embryonic kidney (HEK) 293T cells stably expressing either RHEB-WT or a constitutively active mutant (S16H) of RHEB. Increased mTORC1 signaling, as

evidenced by sustained phosphorylation of S6K1 and its target rpS6, was observed in RHEB-expressing cells (Figure S1B). The activation of the mTORC1 pathway nicely correlated with an increase in glutamine consumption, therefore confirming that changes in mTORC1 signaling are reflected in cellular glutamine uptake (Figure S1B). To determine whether the modulation of glutamine uptake by the mTORC1 pathway occurs in cancer cells, we examined glutamine uptake rates in conditions of mTORC1 inhibition in human epithelial tumor cell lines, including the colon carcinoma DLD1 and the prostate cancer DU145. Rapamycin treatment resulted in decreased proliferation (data not shown) and yielded a decreased glutamine uptake in both cell lines (Figure 1B and data not shown). Glutamine is the major nitrogen donor for the majority of ammonia production in cells (Figure 1C) (Shanware et al., 2011). Consistent with decreased glutamine uptake, we found that ammonia levels were also diminished after rapamycin treatment (Figure S1C).

Next, to examine the fate of glutamine in conditions of mTORC1 inhibition, we used gas chromatography/mass spectrometry (GC/MS) analysis to monitor the incorporation of uniformly labeled [U -¹³C₅]-glutamine into TCA-cycle intermediates. Direct glutamine contribution to α KG (m+5), succinate (m+4), malate (m+4), and citrate (m+4) was decreased in rapamycin-treated cells (Figure S1D), indicating that rapamycin impairs glutamine oxidation and subsequent carbon contribution into the TCA cycle.

To test whether glutamine uptake or glutamine conversion is limiting, we measured the intracellular levels of glutamine and glutamate in DLD1 cells. Increased levels of glutamine and/or glutamate will show that the catalyzing enzyme activity is limiting and not glutamine transport itself (Fendt et al., 2010). Rapamycin treatment resulted in increased intracellular levels of both glutamine and glutamate, showing that glutamate-to- α KG conversion is the critical limiting reaction (Figures 1D and 1E). To further confirm the implication of the glutamate-catalyzing reaction, we also measured α KG levels. If glutamate conversion is indeed critical, we expect no alteration in α KG levels. This is expected because α KG is downstream of the potentially limiting glutamate conversion step, and it has been shown that product metabolite concentrations of limiting metabolic enzymes stay unaltered, whereas the substrate metabolite concentrations change to keep metabolic homeostasis (Fendt et al., 2010). We found that α KG levels were unaltered after rapamycin treatment, corroborating that the limiting enzymatic step is glutamate conversion (Figure 1F). To further confirm the limitation in glutamate-to- α KG conversion, we measured flux through this reaction. Strikingly, this flux was significantly reduced during rapamycin treatment (Figure 1G). Additionally, the inhibition of mTORC1 resulted in increased glutamate secretion (Figure 1H), thus confirming that the glutamate-to- α KG conversion step is a major bottleneck in the glutamine pathway during rapamycin treatment.

Glutamate conversion can be conducted by GDH (Figure 1C), suggesting that the mTORC1 pathway potentially regulates this enzyme. In agreement, rapamycin treatment resulted in decreased GDH activity in DLD1 cells (Figure 1I). To exclude that transaminases play a role in the mTORC1-induced regulation of glutamine metabolism, we used aminooxyacetate (AOA)

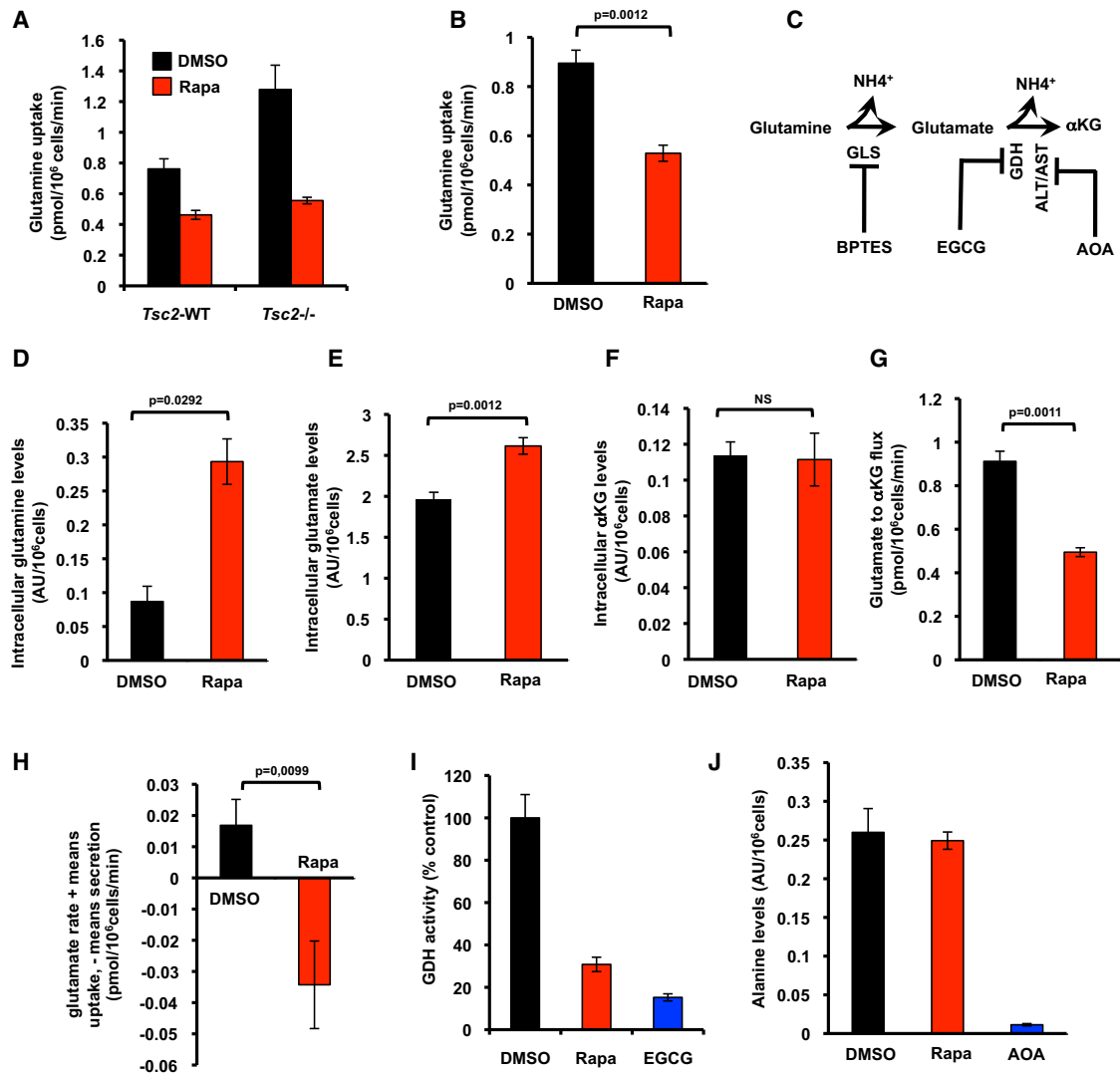


Figure 1. The mTORC1 Pathway Regulates Glutamine Metabolism via GDH

(A and B) Glutamine uptake was determined in (A) *Tsc2*-WT and *Tsc2*^{-/-} MEFs treated with rapamycin and (B) DLD1 cells treated with rapamycin.

(C) A diagram showing the enzymes involved in glutamine anaplerosis and the inhibitors used in this study (see text for more details).

(D–F) Intracellular levels of glutamine (D), glutamate (E), and αKG (F) in DLD1 cells treated with rapamycin.

(G) Glutamate-to-αKG flux was determined in DLD1 cells treated with rapamycin.

(H) Glutamate secretion rates in DLD1 cells treated as in (B).

(I) GDH activity in DLD1 cells treated with rapamycin. EGCG was used as a positive control.

(J) Alanine levels were determined in DLD1 cells treated with rapamycin or AOA.

AU: arbitrary units. The mean is shown; error bars represent SEM (n > 3). See also Figure S1.

at a concentration shown to effectively inhibit the two predominant transaminases, alanine aminotransferase (ALT) and aspartate aminotransferase (AST) (Figure 1C) (Wise et al., 2008), or rapamycin in the presence of α-¹⁵N-labeled glutamine. Subsequently, we measured ¹⁵N-labeling patterns and metabolite levels of alanine, an amino acid that is predominately produced by a transaminase-catalyzed reaction (Possemato et al., 2011). We found that AOA dramatically decreased ¹⁵N contribution and metabolite levels of alanine, whereas rapamycin only mildly affected the ¹⁵N contribution to this amino acid and showed no effect on alanine levels compared to the control condition

(Figures 1J and S1E). In conclusion, these data demonstrate that GDH, not transaminases, plays a major role in the regulation of glutamine metabolism downstream of mTORC1.

mTORC1 Controls GDH Activity by Repressing SIRT4

As our results show that mTORC1 regulates GDH, we sought to identify the molecular mechanism. SIRT4 is a negative regulator of GDH activity through ADP-ribosylation (Haigis et al., 2006), thus suggesting that mTORC1 potentially controls this step of glutamine metabolism via SIRT4. To test this possibility, we first assessed the ADP-ribosylation status of GDH by introducing

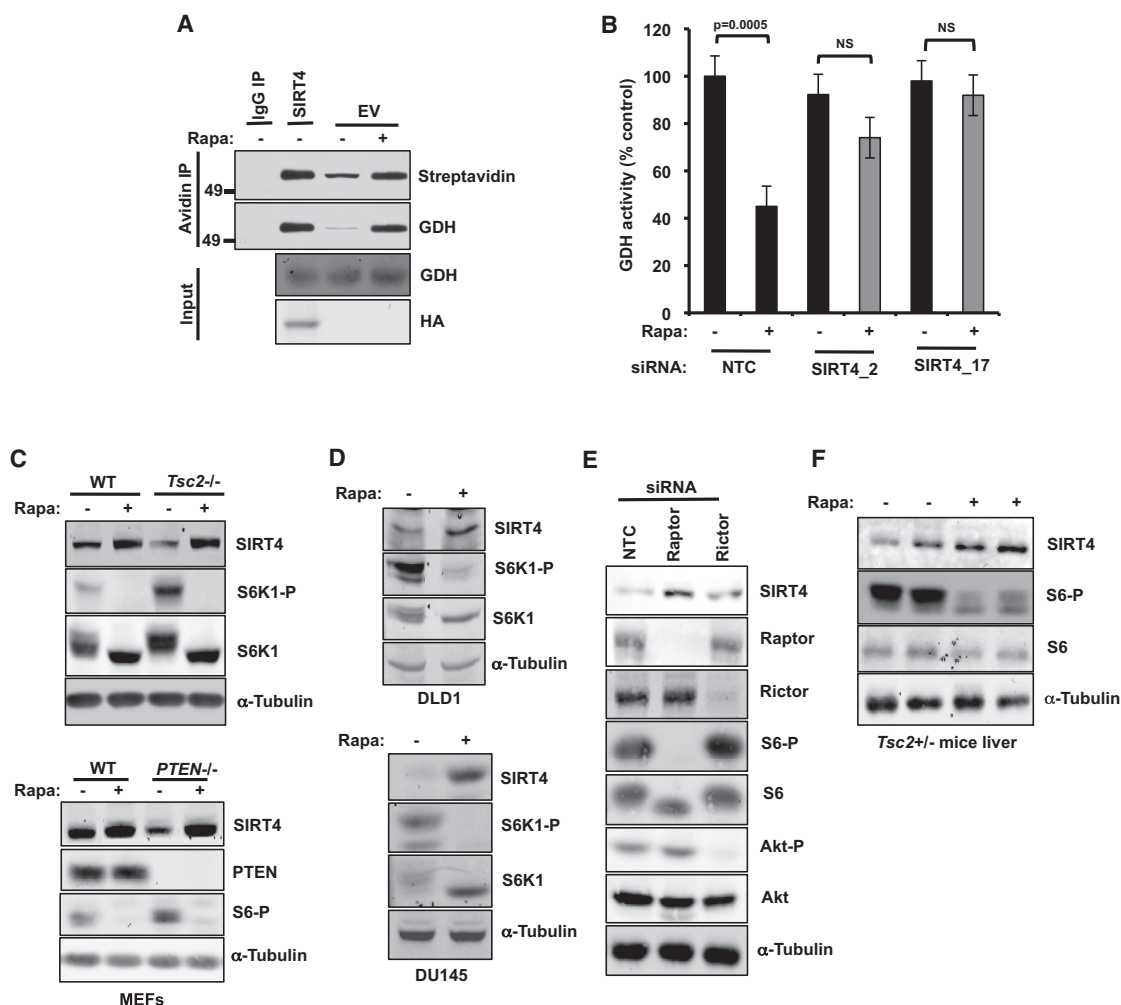


Figure 2. mTORC1 Controls Glutamate Dehydrogenase Activity by Repressing SIRT4

(A) DLD1 cells were treated with rapamycin followed by analysis of mono-ADP-ribosylated GDH as described in the [Experimental Procedures](#). DLD1 cells stably expressing SIRT4-HA were used as a positive control.

(B) GDH activity was determined in *Tsc2*^{-/-} MEFs transfected with a nontargeting control siRNA (NTC) or two independent siRNAs against SIRT4, then treated with rapamycin for 24 hr.

(C–F) SIRT4 protein levels in whole-cell lysates from (C) *Tsc2*-WT, *Tsc2*^{-/-} MEFs and *PTEN*-WT, *PTEN*^{-/-} MEFs treated as in (A); (D) DLD1 and DU145 cells treated as in (A); (E) *Tsc2*^{-/-} MEFs transfected with a nontargeting control (NTC) siRNA or siRNAs targeting either raptor or rictor; and (F) the liver of *Tsc2*^{+/-} mice treated with rapamycin.

The mean is shown; error bars represent SEM ($n > 3$). See also [Figure S2](#).

biotin-labeled NAD followed by immunoprecipitation with avidin-coated beads. Rapamycin treatment led to an increase in the mono-ADP-ribosylation status of GDH, similar to that observed in cells stably expressing SIRT4 ([Figure 2A](#)). Importantly, we found that the knockdown of SIRT4 abrogated the rapamycin-induced decrease in the activity of GDH ([Figures 2B and S2A](#)). Strikingly, SIRT4 protein levels were increased upon mTORC1 inhibition in MEFs ([Figure 2C](#)). This regulation was confirmed in both DLD1 and DU145 cells ([Figure 2D](#)). Remarkably, rapamycin potently increased SIRT4 levels after 6 hr of treatment ([Figure S2B](#)), correlating with reduced glutamine consumption at the same time point (data not shown). In contrast, SIRT4 levels were not influenced by the treatment of MEFs with U0216, an

inhibitor of MEK1/2 in the MAPK pathway ([Figure S2C](#)). All other mTOR catalytic inhibitors tested in *Tsc2*^{-/-} MEFs also resulted in increased SIRT4 protein levels ([Figure S2D](#)). To evaluate a potential regulation of SIRT4 by mTORC2, we performed RNA interference (RNAi) experiments of either raptor or the mTORC2 component rictor in *Tsc2*^{-/-} MEFs. The knockdown of raptor, but not rictor, was sufficient to increase SIRT4 protein levels, confirming the role of the mTORC1 pathway in the regulation of SIRT4 ([Figure 2E](#)). To investigate whether mTORC1 regulation of SIRT4 occurs in tumor samples, a TSC-xenograft model was used. We injected the *TSC2*^{-/-} rat leiomyoma cell line ELT3 expressing either an empty vector (V3) or TSC (T3) in the flank of nude mice. SIRT4 levels were dramatically increased in

TSC2-expressing tumors compared to empty vector samples (Figure S2E). In addition, we assessed the levels of SIRT4 in both ELT3 xenograft tumors and mouse *Tsc2*^{-/-} liver tumors after rapamycin treatment. As expected, these tumor samples exhibited robust elevation of SIRT4 after rapamycin treatment (Figures 2F and S2F). Thus, these data demonstrate that the mTORC1 pathway represses SIRT4 in several tumor systems.

CREB2 Regulates the Transcription of SIRT4 in an mTORC1-Dependent Fashion

We next asked whether the mTORC1-dependent regulation of SIRT4 occurred at the mRNA level. Quantitative RT-PCR results show that rapamycin treatment significantly increased the expression of *SIRT4* messenger RNA (mRNA) in *Tsc2*^{-/-} MEFs (Figure 3A). *SIRT4* mRNA levels were dramatically reduced in *Tsc2*^{-/-} MEFs compared to their WT counterpart (Figure 3B). Similar results were obtained from transcriptional profiling analysis of the *SIRT4* gene from a previously published data set (GSE21755) (Figure 3C) (Düvel et al., 2010). Altogether, our data demonstrate that mTORC1 negatively regulates the transcription of *SIRT4*.

To identify candidate transcription factors regulating *SIRT4*, we analyzed the nucleotide sequence of the human *SIRT4* promoter region. We used the TFSEARCH program, a computer algorithm available at <http://mbs.cbrc.jp/research/db/TFSEARCH.html>, and identified 21 potential transcription factors that may bind directly to and modulate *SIRT4* promoter activity (see Table S1). Interestingly, among these potential hits, CREB2 is involved in the control of many metabolic processes, including glucose, lipid, and amino acid metabolism (Yoshizawa et al., 2009; Wang et al., 2010a; Ye et al., 2010). Moreover, a sequence in the human *SIRT4* promoter displayed significant homology with the canonical CREB recognition motif TGAY-GYAA (Y = C or T) (Figure 3D). To determine whether CREB2 is involved in the mTORC1-dependent regulation of *SIRT4*, we performed RNAi experiments. The silencing of CREB2 abolished the rapamycin-induced expression of *SIRT4* (Figures 3E and S3A). Remarkably, the knockdown of CREB1 did not affect the upregulation of *SIRT4* upon mTORC1 inhibition, thus demonstrating the specificity of CREB2 to induce *SIRT4* (Figure S3B). Moreover, the knockdown of CREB2 significantly abrogated the rapamycin-induced increase in the activity of the *SIRT4* promoter, as determined by using a pGL3 luciferase reporter containing the putative CREB2-binding sequence (Figure 3F). Finally, chromatin immunoprecipitation (ChIP) assays revealed that CREB2 binds *SIRT4* during conditions of mTORC1 inhibition (Figure 3G).

mTORC1 Regulates the Stability of CREB2

We next investigated whether the mTORC1 pathway regulates CREB2. Although we did not observe major changes in *Creb2* mRNA in normal growth conditions (Figure S4A), mTORC1 inhibition resulted in accumulation of CREB2 protein levels by 2 hr of rapamycin treatment (Figure 4A). U0126 failed to cause the accumulation of CREB2 (Figure S4B). In contrast, CREB1 protein levels were not affected after 24 hr of rapamycin treatment (Figure S4C). As observed for SIRT4, mTOR catalytic inhibitors, and the specific knockdown of mTOR, resulted in upregulation of CREB2 protein levels (Figures S4D and S4E). CREB2 is upregu-

lated in diverse cell types as a response to a variety of stresses, including hypoxia, DNA damage, and withdrawal of GFs, glucose, and aa (Chérasse et al., 2007; Rouschop et al., 2010; Yamaguchi et al., 2008; Whitney et al., 2009). Interestingly, mTORC1 is negatively regulated by all of these environmental inputs (Zoncu et al., 2011). Because mTORC1 signaling in *Tsc2*^{-/-} MEFs is insensitive to serum deprivation, we assessed the role of aa withdrawal and restimulation on CREB2 levels. As shown in Figure 4B, CREB2 accumulated upon aa deprivation and was decreased following aa readdition. This phenomenon required the action of the proteasome as MG132 efficiently blocked CREB2 degradation following aa readdition. Importantly, we found that mTORC1 inhibition abrogated the aa-induced decrease of CREB2 (Figure 4B). Similarly, MG132 protected CREB2 levels after insulin stimulation in *Tsc2*-WT MEFs (Figure S4F). These data suggest that mTORC1 regulates the stability of the CREB2 protein in our model. Consistent with this, cycloheximide (CHX) treatment revealed that the increase in CREB2 abundance following mTORC1 inhibition is due to increased CREB2 half-life (Figure 4C). Taken together, our data demonstrate that CREB2 accumulation following mTORC1 inhibition primarily occurs through a posttranscriptional mechanism.

mTORC1 Activation Promotes the Binding of CREB2 to β TrCP and Modulates CREB2 Ubiquitination

Next, we attempted to identify the E3 ubiquitin ligase that might be responsible for CREB2 turnover. Consistent with a recent study, we found CREB2 to bind the E3 ligase β TrCP (Frank et al., 2010). However, other related E3 ligases including Fbxw2, Fbxw7a, and Fbxw9 did not bind to CREB2 (data not shown). The interaction of CREB2 with Flag- β TrCP1 was enhanced in the presence of insulin and was abolished by rapamycin pretreatment (Figure 4D). Importantly, insulin treatment promoted the ubiquitination of CREB2 in an mTORC1-dependent fashion (Figure 4E). Altogether, our results support the notion that the mTORC1 pathway regulates the targeting of CREB2 for proteasome-mediated degradation. β TrCP binds substrates via phosphorylated residues in conserved degradation motifs (degrons), typically including the consensus sequence DpSGX(n)pS or similar variants. We found an evolutionarily conserved putative β TrCP-binding site (DSGXXXS) in CREB2 (Figure 4F). Interestingly, we noted a downward mobility shift in CREB2 protein with mTORC1 inhibition, consistent with a possible decrease in the phosphorylation of CREB2 (Figure 4A). Frank et al. (2010) showed that phosphorylation of the first serine in the degron motif corresponding to Ser218 is required for the CREB2/ β TrCP interaction, and this modification acts as a priming site for a gradient of phosphorylation events on five proline-directed residue codons (T212, S223, S230, S234, and S247) that is required for CREB2 degradation during the cell-cycle progression (Frank et al., 2010). Consistent with these observations, we found that the mutation of the five residues to alanine (5A mutant) resulted in strong stabilization of CREB2, comparable to the serine-to-alanine mutation on the priming Ser218 phosphorylation site (Figure S4G). Single point mutations on each residue did not significantly increase stability compared with CREB2-WT (data not shown). Finally, to confirm the role of these five residues in the regulation of SIRT4, we expressed

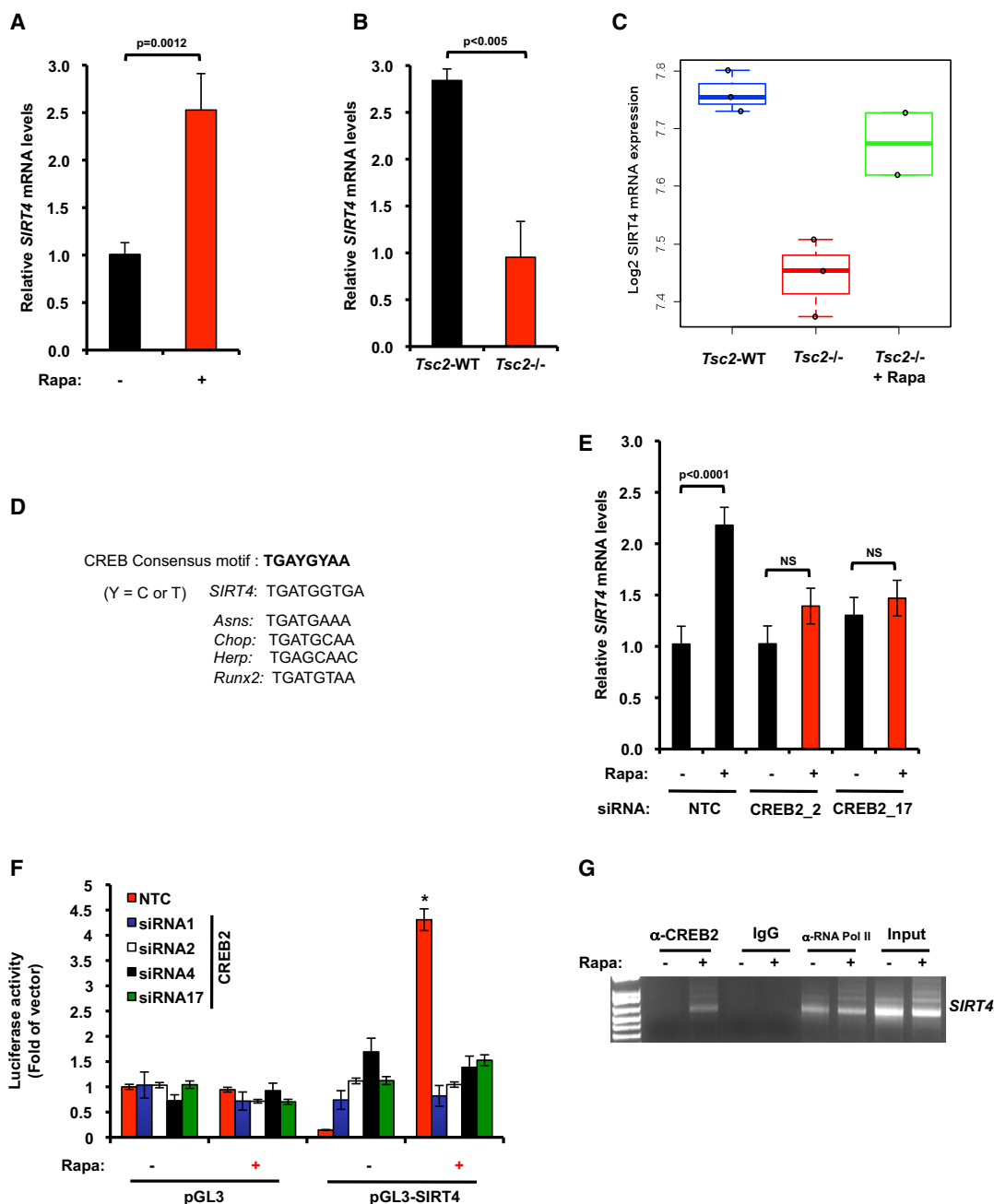


Figure 3. SIRT4 Is Regulated at the mRNA Level in an mTORC1-Dependent Fashion

(A) *SIRT4* mRNA levels in *Tsc2*^{-/-} MEFs treated with rapamycin for 24 hr.

(B) *SIRT4* mRNA levels in *Tsc2*^{-/-} and *Tsc2*-WT MEFs as in (A).

(C) Boxplots of *SIRT4* expression in *Tsc2*-WT (blue) and *Tsc2*^{-/-} MEFs without (red) or with (green) rapamycin treatment.

(D) CREB-binding consensus motif identified on several CREB target gene promoters and the human *SIRT4* gene promoter. The putative CREB recognition sequence on the human *SIRT4* promoter was aligned with other established CREB recognition sequences.

(E) *SIRT4* mRNA levels in *Tsc2*^{-/-} MEFs transfected with nontargeting siRNA (NTC) or with two independent siRNAs against CREB2. Cells were treated with rapamycin for 24 hr.

(F) Normalized luciferase light units of CREB2 knocked down *Tsc2*^{-/-} transfected with a pGL3-luciferase reporter construct or with pGL3-SIRT4. Twenty-four hours after transfection, cells were treated with DMSO or rapamycin for 24 hr (* $p < 0.05$).

(G) *Tsc2*^{-/-} MEFs were incubated in the presence or absence of rapamycin and were then harvested for ChIP analysis with an anti-CREB2 antibody or preimmune IgG. Specific primers were used to amplify *SIRT4*. Input chromatin was diluted to 1:1000. α -RNA polymerase II (Pol II) was used as a positive control. All PCR products were resolved by 2% agarose electrophoresis.

The mean is shown; error bars represent SEM ($n > 3$). See also Figure S3.

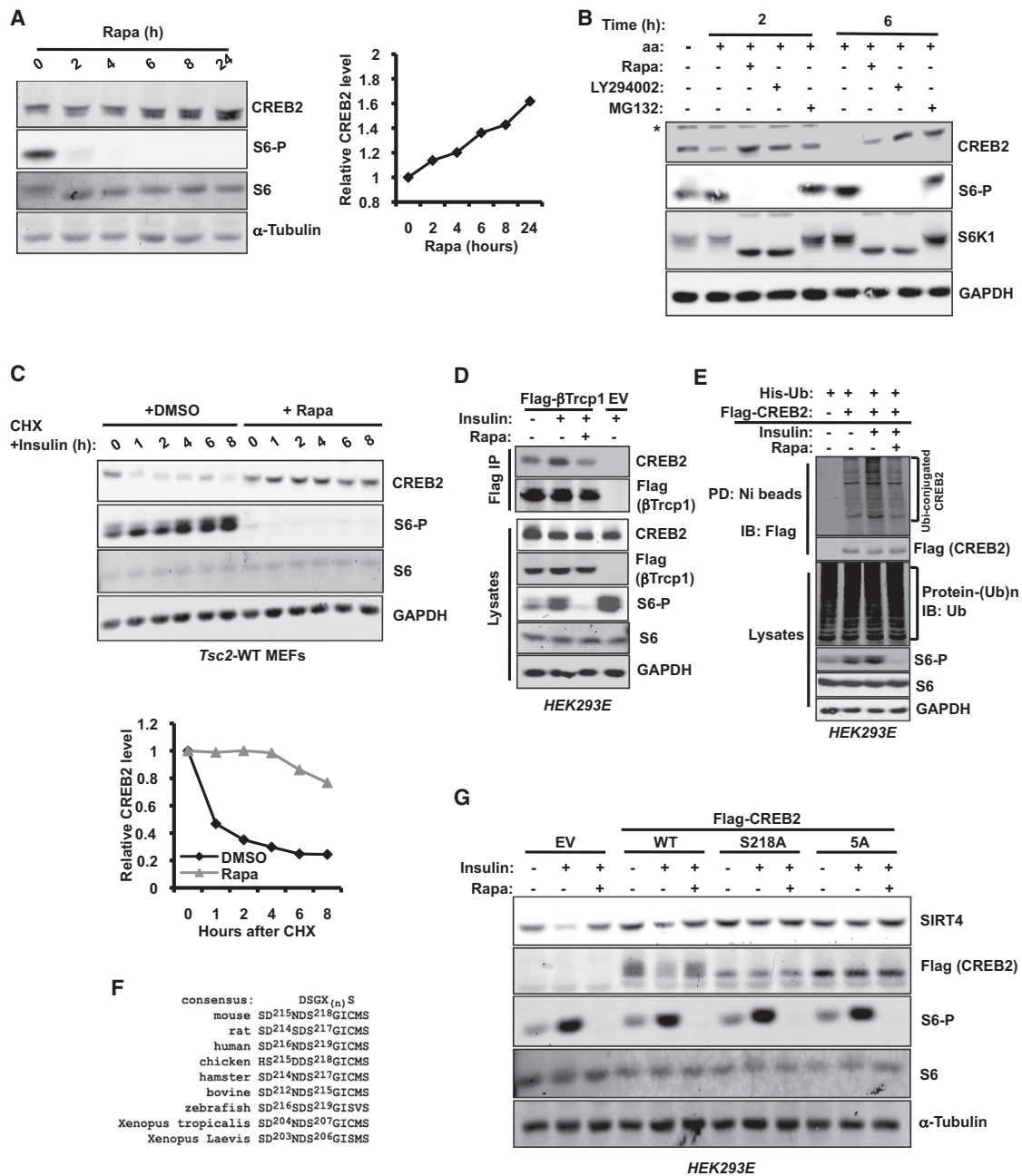


Figure 4. mTORC1 Regulates the Stability of CREB2

(A) Immunoblot analysis of CREB2 in *Tsc2*^{-/-} MEFs treated with rapamycin. Cells were harvested at the indicated time points. The right panel shows the quantification of band intensities. CREB2 bands were normalized to α -tubulin, then normalized to the t = 0 time point.

(B) *Tsc2*^{-/-} MEFs were amino acid (aa) and serum starved for 18 hr and pretreated with the indicated drugs for 30 min, followed by addition of aa for 2 or 6 hr. Protein lysates were resolved by immunoblot with the antibodies indicated. The asterisk (*) denotes a nonspecific band.

(C) *Tsc2*-WT MEFs were serum starved for 18 hr and were pretreated with rapamycin or DMSO for 30 min. One hundred nanomoles of insulin with 20 μ g/ml cycloheximide (CHX) were added to cells before harvesting. The bottom panel shows the quantification of band intensities. CREB2 bands were normalized to GAPDH, then normalized to the t = 0 time point.

(D) HEK293E cells were transfected with constructs coding for Flag- β TrCP1. Twenty-four hours after transfection, cells were serum starved for 18 hr and pretreated with rapamycin for 30 min. One hundred nanomoles of insulin were then added to cells for 2 hr. Total protein lysates were subjected to immunoprecipitation with anti-Flag M2 antibody.

(E) Flag-CREB2 was expressed in HEK293E cells together with His-Ub. Cells were serum starved for 18 hr and treated with MG132 for 4 hr. Then, cells were pretreated with either DMSO or rapamycin for 30 min. One hundred nanomoles of insulin were added for 6 hr. His-ubiquitinated proteins were pulled down with Ni-NTA agarose and analyzed by immunoblotting.

(legend continued on next page)

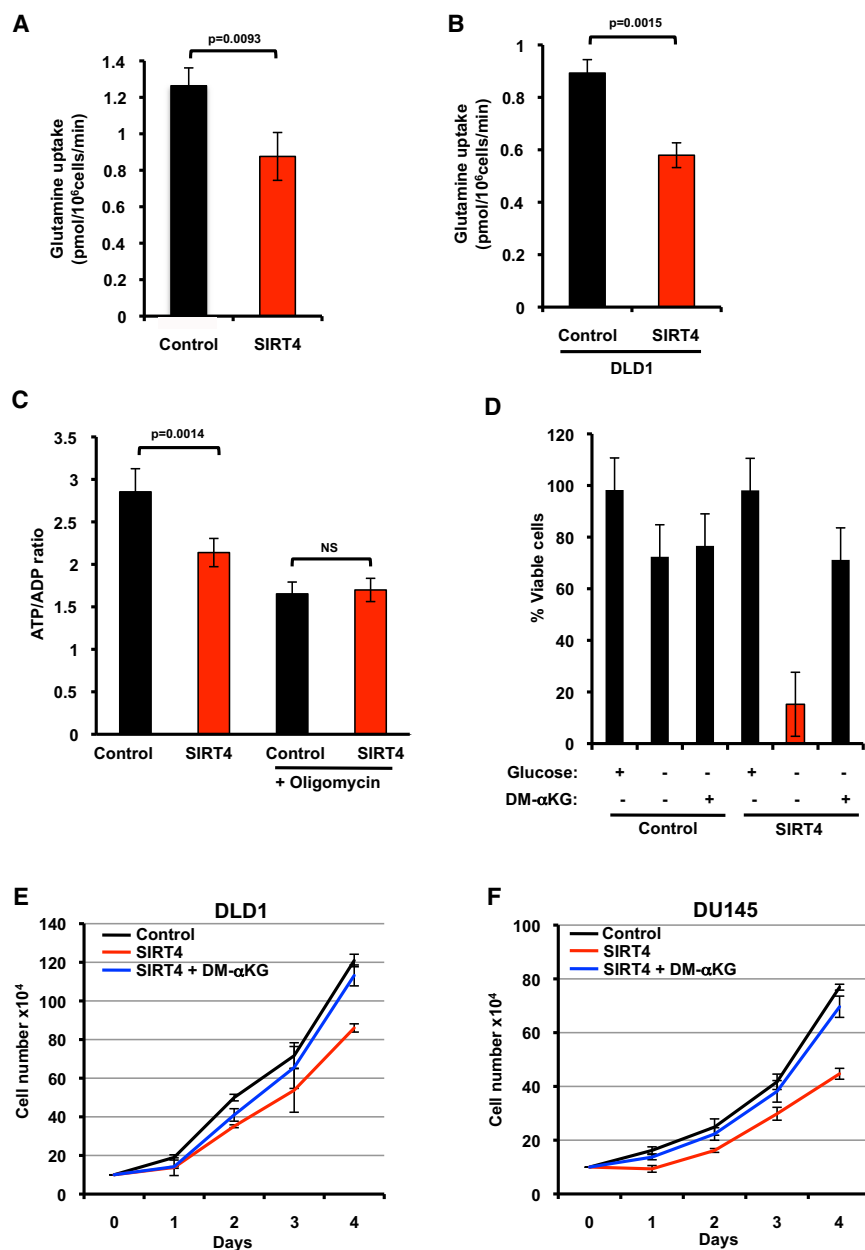


Figure 5. SIRT4 Represses Bioenergetics and Proliferation

(A and B) Glutamine uptake was determined in (A) *Tsc2*^{-/-} MEFs stably expressing SIRT4 or vector control and (B) DLD1 cells expressing SIRT4 or vector control.

(C) The ATP/ADP ratio was measured in *Tsc2*^{-/-} control or SIRT4-expressing MEFs treated with or without oligomycin (5 μ g/ml).

(D) Cell viability of control or SIRT4-expressing *Tsc2*^{-/-} MEFs deprived of glucose and supplemented with DM- α KG (7 mM) or pyruvate (1 mM) for 48 hr.

(E and F) Growth curves of DLD1 (E) and DU145 (F) cells stably expressing SIRT4 or vector control. Cells were cultured in standard media lacking pyruvate, and DM- α KG was added to media as indicated. Cell number was measured every 24 hr for 4 consecutive days.

The mean is shown; error bars represent SEM (n > 3). See also Figure S5.

our results demonstrate that the mTORC1 pathway promotes the destabilization of CREB2 to downregulate *SIRT4* expression.

SIRT4 Represses Bioenergetics and Cell Proliferation

We observed that glutamine utilization is repressed by rapamycin treatment (Figure 1), and SIRT4 is induced by mTORC1 inhibition (Figure 2). Thus, we tested whether SIRT4 itself directly regulates cellular glutamine uptake. The stable expression of SIRT4 resulted in the repression of glutamine uptake in *Tsc2*^{-/-} MEFs and DLD1 cells (Figures 5A and 5B). Glucose uptake was not affected by SIRT4 expression (data not shown). Because glutamine can be an important nutrient for energy production, we examined ATP levels in SIRT4-expressing cells. Consistent with reduced glutamine consumption, the expression of SIRT4 in *Tsc2*^{-/-} cells resulted in a decreased

ATP/ADP ratio compared to control cells (Figure 5C). Cells produce ATP via glycolysis and oxidative phosphorylation (OXPHOS). To test the contribution of mitochondrial metabolism versus glycolysis to ATP, we measured the ATP/ADP ratio after the treatment with oligomycin, an inhibitor of ATP synthesis from OXPHOS. Importantly, the difference of the ATP/ADP ratio between control and SIRT4-expressing cells was abrogated by oligomycin (Figure 5C), further demonstrating that SIRT4 may

Flag-CREB2-WT, S218A, and 5A in serum-starved HEK293E. As shown in Figure 4G, insulin addition to cells expressing an empty vector (EV) resulted in decreased SIRT4 levels, a phenomenon abrogated by rapamycin pretreatment. SIRT4 levels were upregulated in cells expressing Flag-CREB2-WT, S218A, and 5A when compared to control cells. However, only the expression of either S218A and 5A mutants was able to block the insulin-mediated decrease of SIRT4 (Figure 4G). Taken together,

(F) Schematic of the conserved β TrCP degrons in CREB2 across multiple species.

(G) CREB2 mutants were expressed in HEK293E cells. These cells were serum starved for 18 hr and pretreated with rapamycin for 30 min. One hundred nanomoles of insulin were added to the media for 8 hr.

See also Figure S4.

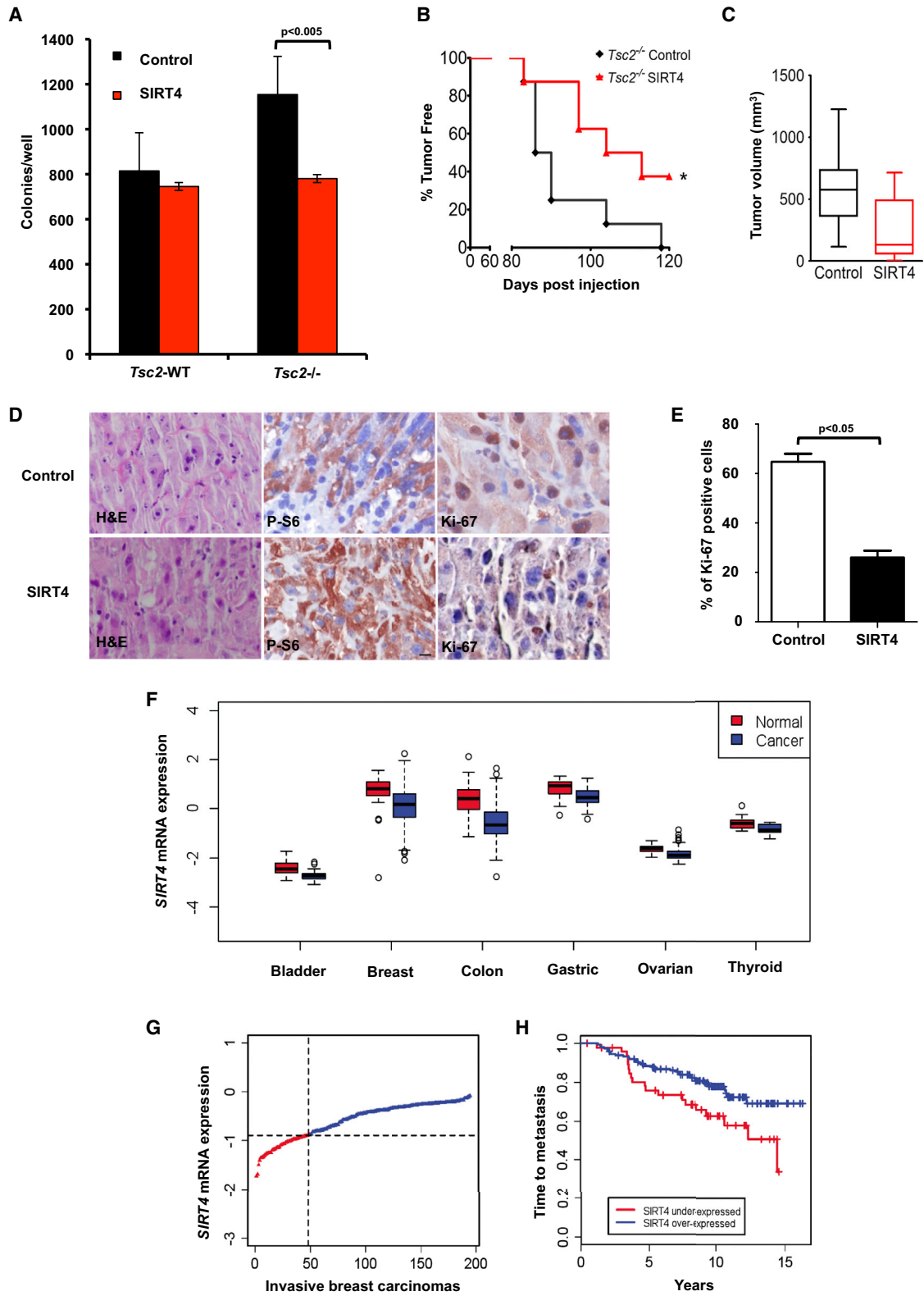


Figure 6. SIRT4 Suppresses TSC-Tumor Development

(A) Soft agar assays with *Tsc2*^{-/-} or *Tsc2*-WT MEFs expressing control vector or SIRT4.

(B) Kaplan-Meier plot of the percentage of tumor-free mice after inoculation with *Tsc2*^{-/-} *p53*^{-/-} MEFs expressing control or SIRT4 vectors (n = 8). *p < 0.05.

(legend continued on next page)

repress the ability of cells to generate energy from mitochondrial glutamine catabolism.

Mitochondrial glutamine catabolism is essential for energy production and viability in the absence of glucose (Yang et al., 2009; Choo et al., 2010). Thus, we examined the effect of SIRT4 on the survival of *Tsc2*^{-/-} MEFs during glucose deprivation. Control cells remained viable following 48 hr of glucose deprivation. Conversely, SIRT4-expressing cells showed a dramatic increase in cell death under glucose-free conditions, and this increase was rescued by the addition of the cell-permeable dimethyl- α KG (DM- α KG) (Figure 5D). In contrast, the expression of SIRT4 did not affect the viability of glucose-deprived *Tsc2*-WT MEFs (Figure S5A). Glucose deprivation also induced death of the human DU145 cancer cell line stably expressing SIRT4 (data not shown).

Glutamine is an essential metabolite for proliferating cells, and many cancer cells exhibit a high rate of glutamine consumption (DeBerardinis et al., 2007). Thus, decreased glutamine uptake in DLD1 and DU145 cancer cells expressing SIRT4 might result in decreased proliferation. Indeed, these cells grew significantly slower than did control cells. Remarkably, DM- α KG completely abrogated the decreased proliferation of SIRT4-expressing cells (Figures 5E and 5F), suggesting that repressed glutamine metabolism drove the reduced proliferation of cells expressing SIRT4. The expression of SIRT4 also slowed the proliferation of *Tsc2*^{-/-} MEFs but did not affect *Tsc2*-WT MEFs (Figures S5B and S5C). Finally, to rule out that the effect on proliferation was due to aberrant localization and to off-target effects of the overexpressed protein, we examined the localization of HA-SIRT4. We found that SIRT4 is colocalized with the MitoTracker, a mitochondrial-selective marker (Figure S5D). Taken together, these data demonstrate that SIRT4 is a critical negative regulator of mitochondrial glutamine metabolism and cell proliferation.

SIRT4 Represses TSC-Tumor Development

Recent studies have demonstrated a major role of glutamine metabolism in driving oncogenic transformation of many cell lines (Gao et al., 2009; Wang et al., 2010b). Because SIRT4 expression represses glutamine uptake and cell proliferation (Figure 5), we hypothesized that it could affect tumorigenesis. To test this idea, we used an anchorage-independent growth assay to assess the role of SIRT4 in cell transformation. SIRT4 expression reduced the ability of *Tsc2*^{-/-} *p53*^{-/-} MEFs to grow in soft agar. However, the expression of SIRT4 in *Tsc2*^{+/+} *p53*^{-/-} did not impair their colony-formation properties (Figure 6A). Next, we performed xenograft assays to investigate the impact of SIRT4 in cell growth in vivo. We inoculated *Tsc2*^{-/-} *p53*^{-/-} and *Tsc2*^{+/+} *p53*^{-/-} MEFs stably expressing SIRT4 or vector control,

subcutaneously and bilaterally, into nude mice (n = 8 per group). Tumor incidence in mice injected with *Tsc2*^{+/+} *p53*^{-/-} MEFs was not affected by SIRT4 (data not shown). Conversely, in the *Tsc2*^{-/-} *p53*^{-/-} cohort, SIRT4 reduced tumor incidence by 20 days at median (Figure 6B). Furthermore, at post-inoculation day 80, mice injected with SIRT4 cells had a mean tumor volume of 246.1 \pm 124.1 mm³, whereas mice injected with control cells had a mean tumor volume of 589.1 \pm 101.5 mm³ (p < 0.05) (Figure 6C). As expected, SIRT4 and control tumors were immunoreactive for phospho-S6 (Figure 6D) and expressed HA-SIRT4 (Figure S6). Furthermore, SIRT4 expression in *Tsc2*^{-/-} *p53*^{-/-} MEFs resulted in reduction of Ki-67 positivity by 60% (Figure 6E), consistent with the finding that SIRT4 inhibits the proliferation of these cells in vitro (Figure S5B). Finally, we performed a comprehensive meta-analysis of *SIRT4* expression in human tumors and found significantly lower expression levels of *SIRT4*, relative to normal tissue, in bladder, breast, colon, gastric, ovarian, and thyroid carcinomas (Figure 6F). Interestingly, loss of *SIRT4* expression showed a strong association with shorter time to metastasis in patients with breast cancer (Figures 6G and 6H). Altogether, these data strongly suggest that SIRT4 delays tumorigenesis regulated by the mTORC1 pathway.

The Pharmacologic Inhibition of Glutamine Anaplerosis Synergizes with Glycolytic Inhibition to Induce the Specific Death of mTORC1-Hyperactive Cells

The activation of mTORC1 leads to glucose and glutamine addiction as a result of increased uptake and metabolism of these nutrients (Choo et al., 2010; Düvel et al., 2010) (Figure 1). These observations suggest that targeting this addiction offers an interesting therapeutic approach for mTORC1-driven tumors. The alkylating agent, mechlorethamine (Mechlo), incites cell toxicity in part by the inhibition of the GAPDH step of glycolysis via poly-ADP ribose polymerase (PARP)-dependent cellular consumption of cytoplasmic NAD⁺. The ultimate consequence is glycolytic inhibition, thus mimicking glucose deprivation (Zong et al., 2004). Treatment of *Tsc2*^{-/-} MEFs with Mechlo decreased both NAD levels and lactate production (Figure 7A and data not shown). The decrease in NAD⁺ levels was rescued by addition of DPG (Figure 7A), a PARP inhibitor (Zong et al., 2004). We next tested the ability of glutamine inhibition to determine the sensitivity of *Tsc2*^{-/-} MEFs to Mechlo. As shown in Figure 7B, the treatment with EGCG, a GDH inhibitor (Figure 1G), potentially synergized with Mechlo to kill *Tsc2*^{-/-} MEFs with the greatest effect observed at 30 μ M (Figure 7B). As a result, this combination dramatically increased the cleavage of PARP, an apoptotic marker (Figure 7E). Similarly, glutamine deprivation sensitized *Tsc2*^{-/-} MEFs to Mechlo (data not shown). The RNAi-mediated

(C) Tumor volume and weight were measured.

(D) Immunohistochemical analysis of Ki-67 and representative H&E staining (original magnification, 20 \times).

(E) Quantification of Ki-67 staining in tumors from (D).

(F) Boxplots indicating significantly lower expression of *SIRT4* gene in bladder, breast, colon, gastric, ovarian, and thyroid carcinomas compared to corresponding normal ($p < 0.05$).

(G) Ranked *SIRT4* expression in a breast carcinoma data set of 195 tumors.

(H) Kaplan-Meier curve comparing time to metastasis between breast carcinomas with the lowest (<25th percentile) versus highest (>25th percentile) *SIRT4* expression (p = 0.02, log-rank test).

The mean is shown; error bars represent SEM (n > 3). See also Figure S6.

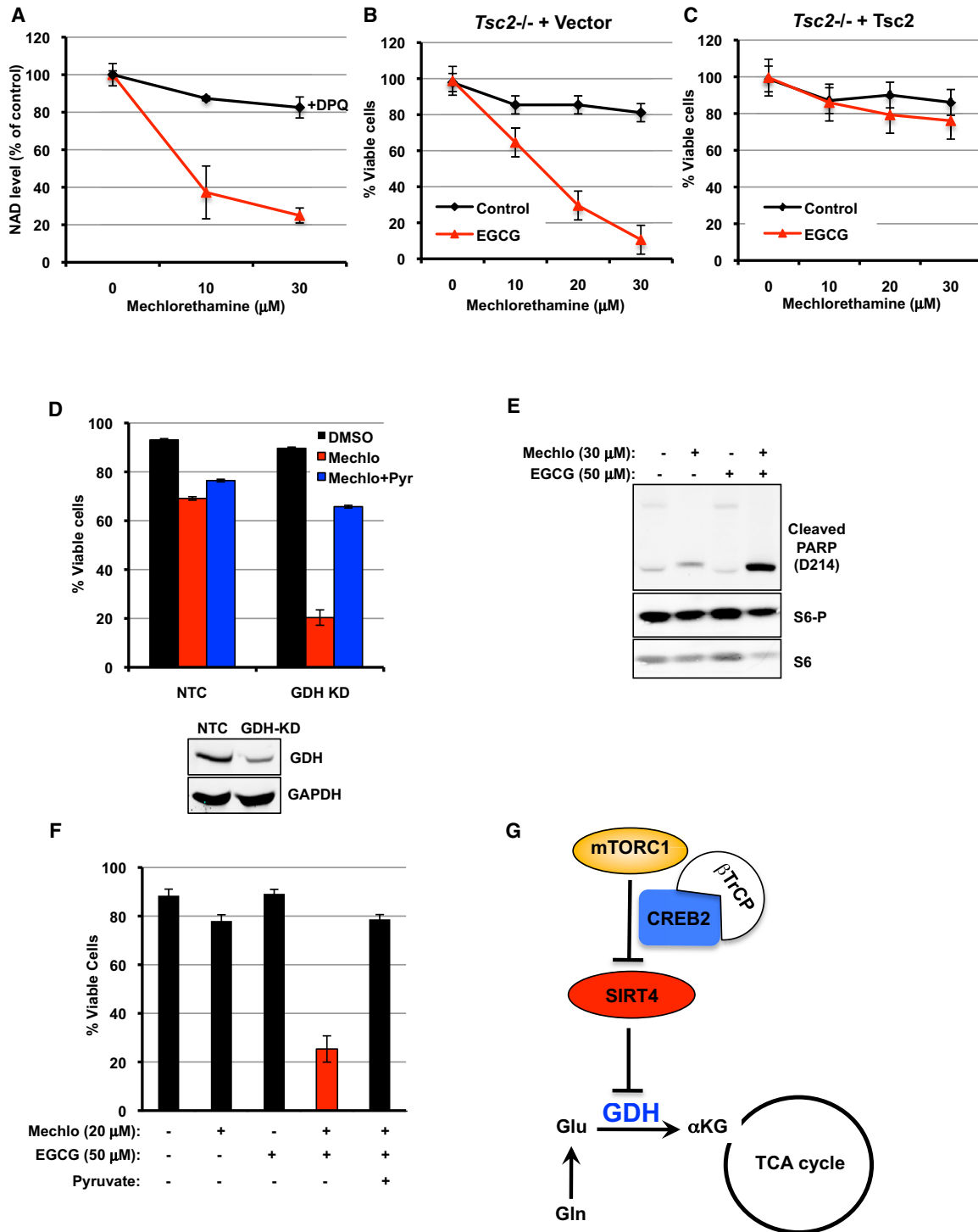


Figure 7. The Combination of Glutamine Metabolism Inhibitors with Glycolytic Inhibition Is an Effective Therapy to Kill *Tsc2*^{-/-} and *PTEN*^{-/-} Cells

(A) NAD levels in *Tsc2*^{-/-} MEFs treated with the indicated doses of mechlorethamine with or without DPQ for 24 hr.
 (B) *Tsc2*^{-/-} MEFs transduced with an empty vector were given the indicated doses of mechlorethamine with or without EGCG (50 μM). Cell viability was measured 48 hr post-treatment via PI exclusion.
 (C) *Tsc2*^{-/-} MEFs re-expressing Tsc2 were treated as in (B).
 (D) *Tsc2*^{-/-} MEFs were transfected with a nontargeting control siRNA (NTC) or siRNA targeting GDH. Twenty-four hours post-transfection, cells were treated with 20 μM of mechlorethamine, and cell viability was determined 48 hr later post-treatment.

(legend continued on next page)

knockdown of GDH also synergized with Mechlo to induce death of *Tsc2*^{-/-} MEFs (Figure 7D). Importantly, at these concentrations, the combination did not induce death of a *Tsc2*-rescued cell line (Figure 7C).

Because the metabolic properties of cells with activated mTORC1 by *Tsc2* deficiency can be efficiently targeted, we also examined other cell types in which mTORC1 is hyperactive by the loss of *PTEN*. We found that the combination of Mechlo and EGCG was also effective in inducing specific toxicity of *PTEN*^{-/-} MEFs, whereas *PTEN*^{+/+} MEFs were not affected (Figures S7A and S7B). In addition, the *PTEN*-deficient human prostate adenocarcinoma cell line LNCaP was also sensitive to treatment with Mechlo and EGCG (Figure 7F). This effect was specifically due to lack of TCA-cycle replenishment as pyruvate supplementation completely reversed the synergistic effect (Figure 7F). The combination of Mechlo with the GLS1 inhibitor BPTES (Figure 1G) also resulted in decreased viability of *Tsc2*^{-/-} cells but not of *Tsc2*-reexpressing cells (Figures S7C and S7D). Again, death in *Tsc2*^{-/-} cells was rescued with pyruvate or OAA (Figure S7E). To further investigate whether the potent cell death in *Tsc2*^{-/-} was restricted to Mechlo, we used 2-DG, a glycolytic inhibitor. The combination of 2-DG with either EGCG or BPTES resulted in enhanced cell death of *Tsc2*^{-/-} MEFs compared to single-agent treatments (Figure S7F). This effect was also specific to *Tsc2*^{-/-} cells, as this combination was less toxic in *Tsc2*-re-expressing MEFs (Figure S7G). Taken together, our results demonstrate that the combination treatments aimed at inhibiting glycolysis and glutaminolysis potently synergize to kill cells with hyperactive mTORC1 signaling.

DISCUSSION

Here, we define an mTORC1-regulated pathway that controls glutamine-dependent anaplerosis and energy metabolism (Figure 7G). We discovered that the mTORC1 pathway regulates glutamine metabolism by promoting the activity of GDH (Figures 1, 2, and 3). We show that this regulation occurs by repressing the expression of *SIRT4*, an inhibitor of GDH (Figures 2 and 3). Molecularly, this is the result of mTORC1-dependent proteasome-mediated degradation of the *SIRT4* transcriptional regulator CREB2 (Figure 4). Interestingly, the modulation of CREB2 levels correlates with increased sensitivity to glutamine deprivation (Ye et al., 2010; Qing et al., 2012), fitting with our model of glutamine addiction as a result of mTORC1 activation (Choo et al., 2010). Our data suggest that mTORC1 promotes the binding of the E3 ligase β TrCP to CREB2 (Figure 4D), promoting CREB2 degradation by the proteasome (Figure 4E). A previous study has demonstrated that five residues in CREB2 located next to the β TrCP degron are required for its stability (Frank et al., 2010). Accordingly, the mutation of these residues to alanine resulted in stabilization of CREB2 and *SIRT4* following insulin- and aa-dependent mTORC1 activation (Figure 4G). Future work is aimed at determining whether mTORC1 and/or

downstream kinases are directly responsible for the multisite phosphorylation of CREB2.

The identification of CREB2 as an mTORC1-regulated transcription factor increases the repertoire of transcriptional regulators, including HIF1 α (glycolysis), Myc (glycolysis), and SREBP1 (lipid biosynthesis), that are modulated by this pathway (Düvel et al., 2010; Yecies and Manning, 2011). The oncogene Myc has also been linked to the regulation of glutamine metabolism by increasing expression of the surface transporters ASCT2 and SN2 and the enzyme GLS. Thus, enhanced activity of Myc correlates with increased glutamine uptake and glutamate production (Wise et al., 2008; Gao et al., 2009). Our findings describe an important level of control to this metabolic node as shown by the modulation of the glutamate-to- α KG flux (Figure 2). This regulation is particularly relevant as some cancer cells produce more than 50% of their ATP by oxidizing glutamine-derived α KG in the mitochondria (Reitzer et al., 1979). Therefore, these studies support the notion that Myc and CREB2/*SIRT4* cooperate to regulate the metabolism of glutamine to α KG. Interestingly, Myc function may also be regulated by mTORC1 (West et al., 1998), although the mechanism is not known. Thus, besides controlling CREB2/*SIRT4*/GDH, mTORC1 might also influence the Myc/GLS axis, explaining the decrease of glutamine uptake observed in rapamycin-treated cells (Figure 1).

Our studies reveal the important impact of *SIRT4* function on glutamine anaplerosis and tumor cell metabolism. Importantly, *SIRT4* expression is decreased in a panel of human cancers, and we show that its expression results in decreased cell transformation and tumor development in a TSC-xenograft model (Figure 6). *SIRT3* also represses tumorigenesis by regulating both genomic instability and the Warburg effect (Kim et al., 2010; Finley et al., 2011). Thus, these two mitochondrial sirtuins seem to function coordinately to modulate cell proliferation by controlling the two major nutrient sources required for tumor cell anabolism.

Glutamine is the main precursor for GSH synthesis despite sufficient glucose and oxygen levels, and the pharmacologic inhibition of GLS results in increased reactive oxygen species (ROS) and decreased proliferation (Le et al., 2012). Therefore, the importance of the glutamine pathway as a substrate for the TCA cycle, or as a regulator of redox homeostasis, may be important for cancer cell adaptation and survival. As a proof of concept, we show that inhibition of glutamine metabolism synergizes with glycolytic attenuation to induce robust death of *Tsc2*^{-/-} cells, whereas their normal counterparts are not sensitive to dual inhibition. EGCG, an antioxidant found in green tea extracts and a potent inhibitor of GDH (Li et al., 2006), is already in several clinical trials as an anticancer agent and has been shown to be effective in limiting tumor growth in mice (Li et al., 2006; Khan and Mukhtar, 2008; Xu et al., 1992; Zhang et al., 2010).

Our findings shed light on potential therapeutic strategies for cancers and genetic disorders, such as TSC and LAM, characterized by deregulation of the mTORC1 pathway. Recently,

(E) Immunoblot analysis of cleaved PARP in *Tsc2*^{-/-} MEFs treated with mechlorethamine (30 μ M) or EGCG (50 μ M) or the combination of both drugs for 24 hr.

(F) Cell viability of LNCaP cells treated with mechlorethamine or EGCG or the combination of both drugs. Pyruvate was added to the media as indicated.

(G) Schematic of the regulation of *SIRT4* and glutamine metabolism by the mTORC1 pathway.

The mean is shown; error bars represent SEM ($n > 3$). See also Figure S7.

rapamycin analogs showed efficacy in reducing the size of angiomyolipomas in clinical trials of TSC (Bissler et al., 2008). Moreover, these agents stabilized respiratory function and were associated with improvement in quality of life of LAM patients (McCormack et al., 2011). However, although the response to rapamycin was significant, effects were cytostatic, and tumor growth was observed after therapy cessation (Bissler et al., 2008), highlighting the need to develop specific agents for therapeutic intervention. TSC tumors display low fluorodeoxyglucose (FDG) uptake in PET scanning (Young et al., 2009), suggesting that a source other than glucose fuels these tumors for survival; glutamine is likely to be such a source. Interestingly, we observed increased cell death of patient-derived LAM cells cultured under glutamine deprivation (data not shown). Therefore, we speculate that targeted inhibition of glutaminolysis may induce tumor cell toxicity in LAM patients.

In sum, our work illustrates that mTORC1 inhibits the activity of GDH by regulating the transcription of *SIRT4*. Moreover, our studies support the rationale of using PET imaging by 4-fluoroglutamine for mapping glutaminolytic tumors (Lieberman et al., 2011) and, importantly, the development of drugs targeting glutamine metabolism as cancer therapy.

EXPERIMENTAL PROCEDURES

Cell Lines and Culture

Tsc2^{-/-} *p53*^{-/-} and *Tsc2*^{+/+} *p53*^{-/-} MEFs were kindly provided by Drs. Brendan Manning and David Kwiatkowski (Harvard Medical School). ELT3 cells were provided by Dr. Cheryl Walker (University of Texas). All other cell lines were obtained from the American Type Culture Collection (ATCC). MEFs, ELT3, HEK293T, and HEK293E cells were cultured in DMEM. DLD1, LNCaPs, and DU145 cells were cultured in RPMI media (Mediatech). DMEM or RPMI were supplemented with 10% FBS (dialyzed for deprivation experiments—GIBCO). All DMEM lacking glucose, aa, L-glutamine, or combinations were made from formulations provided by Sigma. All extra energetic additives that are often added to some DMEM formulations such as sodium pyruvate and succinate were excluded.

Antibodies, Chemicals, and Plasmids

The antibodies used for this study are the following: Ki-67 antibody is from BioGenex. p53, HIF-1 α , Raptor, p70, 389(P) p70, S6(P), Akt-473, Akt, α -tubulin, 4EBP1, PTEN, TSC2, 202(P)204(P) ERK1/2, ERK1/2, 51(P) eIF2 α , CREB, and cleaved PARP were all purchased from Cell Signaling Technologies. Antibody to CREB2 was purchased from Santa Cruz, Inc. Antibody to GDH was purchased from Abcam. SIRT4 and FLAG-M2 were purchased from Sigma. Rictor antibody was from Bethyl Laboratories. GAPDH antibody was purchased from Ambion. PAR antibody was from Calbiochem. The following chemicals were used in this study: rapamycin (Calbiochem), EGCG (Calbiochem), LY294002 (Calbiochem), cycloheximide (Calbiochem), methylpyruvate (Sigma), aminooxyacetate (Sigma), DM- α -ketoglutaric acid (Sigma), sodium pyruvate (Sigma), mechlorethamine hydrochloride (Sigma), succinic acid (Sigma), glutamate (Sigma), U0126 (Selleckchem), 3-methyladenine (Sigma), oligomycin (Calbiochem), insulin (Sigma), PI-103 (Selleckchem), MG132 (Sigma), DPQ (Santa Barbara Technology), biotin-NAD⁺ (Trevigen), lipofectamine and RNAi MAX (Invitrogen), and bromobimane (Sigma). *SIRT4* was cloned into pBabe, *TSC2* was cloned into pLPCX, and the *TSC2*-containing viruses were used to reconstitute *Tsc2*^{-/-} *p53*^{-/-} MEFs. RHEB-WT and S16H were cloned into pLPCX2.

Cell-Number Measurements

Tsc2^{-/-} MEFs were grown on 6-well plates and treated as indicated, trypsinized, and resuspended in PBS (pH 7.2) in a total of 10 ml. Cell number was immediately analyzed on a Z2 Coulter Counter, and results were graphed in Coulter AccuComp Software, gating between 12 μ m and 30 μ m.

Cell-Viability Measurements

All cell-viability experiments were conducted with propidium iodide (PI) exclusion assay. In brief, PI was added to culture media (1 μ g/ml) for 5 min prior to collection. The media from each sample were collected, and then the plates were washed briefly with saline. The saline was added to the media collection tube, and then the remaining cells on the plate were detached with trypsin. The cells were then collected and also put into the original media collection tube. The entire tube, which now had the original media with saline wash and trypsinized cells, was centrifuged, and the pellet was analyzed for PI exclusion via fluorescence-activated cell sorting (FACS) (Beckon Dickinson). Additionally, the cells were washed with media lacking glucose and all amino acids (1/2 volume of incubating media) prior to adding the experimental media, which contained dialyzed FBS. For mechlorethamine experiments, cells were plated overnight (~15–18 hr), and media was changed for new media without pyruvate and with or without glutamine/glucose. Eight hours after the change, cells were given different doses of mechlorethamine.

Cell Lysis and Immunoprecipitations

Cells washed once with cold PBS were solubilized on ice either in a regular lysis buffer (40 mM HEPES [pH 7.4], 1 mM EDTA, 120 mM NaCl, 10 mM β -glycerophosphate, 1 mM NaF, 1 mM Na₃VO₄, and 0.3% CHAPS) or in a low-salt lysis buffer (40 mM HEPES [pH 7.4], 1 mM EDTA, 10 mM β -glycerophosphate, 1 mM NaF, 1 mM Na₃VO₄, and 0.3% CHAPS) supplemented with protease inhibitors (250 μ M PMSF, 5 μ g/ml pepstatin A, 10 μ g/ml leupeptin, and 5 μ g/ml aprotinin). Cleared cell lysates were obtained by centrifugation at 10,000 rpm for 10 min at 4°C, and 0.7–1.2 mg of the lysates were used for immunoprecipitations. For this, cell lysates were incubated with primary antibodies for 2 hr at 4°C followed by 1–2 hr of further incubation with 50% slurry of protein A/G-sepharose presaturated with the lysis buffer. After rinsing three times with the regular or low-salt lysis buffer, immunoprecipitated proteins were recovered from the beads by boiling for 10 min in sample buffer and analyzed by immunoblotting.

Labeling, Flux, and Metabolite-Level Measurements

Labeled tissue cultures were washed with saline, and metabolism was quenched with -20°C cold 65% methanol. After cell scraping in 65% methanol, -20°C cold chloroform was added, and the samples were vortexed at 4°C to extract metabolites. Phase separation was achieved by centrifugation at 4°C. Methanol phase was separated and dried by applying constant airflow. Dried metabolite samples were stored at -80°C .

Metabolites were derivatized with methoxyamine (TS-45950 Thermo Scientific) for 90 min at 40°C and subsequently with N-(tert-butylidimethylsilyl)-N-methyl-trifluoroacetamide, with 1% tert-butylidimethylchlorosilane (375934-Sigma) for 60 min at 60°C. Isotopomer distributions and metabolite levels were measured with a 6890N GC system (Agilent Technologies) combined with a 5975B Inert XL MS system (Agilent Technologies). Isotopomer distributions were analyzed with the Matlab-based software Metran (Antoniewicz et al., 2007). Total ion counts were normalized with the internal standard norvaline and cell number to yielded metabolite levels. Glutamate-to- α KG flux was calculated based on glutamine and glutamate uptake or secretion rates.

NAD Measurement

To measure NAD levels, we used the NAD/NADH kit from Abcam (ab65348) according to the manufacturer's instructions.

In Vivo Manipulations

Two million *Tsc2*^{-/-} *p53*^{-/-} or *Tsc2*^{+/+} *p53*^{-/-} MEFs stably expressing SIRT4-HA or vector control pBabe were inoculated bilaterally into the posterior back region of 6- to 8-week-old immunodeficient CD-1 nude mice (Taconic). Tumor length, width, and depth were measured with a Vernier caliper by an investigator blinded to the experimental conditions. 2.5 million V3 or T3 ELT3 cells were inoculated bilaterally into the posterior back region of 6-week-old immunodeficient CB17 SCID mice (Taconic). Tumors were harvested when they reached 150 mm². Seven-month-old *Tsc2*^{-/-} mice in A/J background were treated with either vehicle or rapamycin (Biomol) at a dose of 6 mg/kg every other day for 3 days (two injections) (Figure 2F).

2.5 million ELT3 cells were inoculated bilaterally into the posterior back region of 6-week-old immunodeficient CB17 SCID mice (Taconic). When tumors reached 100 mm², mice were randomly assigned to intraperitoneal (i.p.) rapamycin (Biomol) at a dose of 1 mg/kg or sterile PBS three times per week for 2 weeks (Figure S2F). The animal studies were approved by the Animal Care and Use Committee of Children's Hospital, Boston.

Statistics

Data were expressed as average \pm standard error of the mean (SEM) of at least three independent experiments. An unpaired, two-tailed Student's *t* test was used to determine differences between two groups. For the tumor incidence study, statistical analyses were performed using the log-rank (Mantel-Cox).

SUPPLEMENTAL INFORMATION

Supplemental Information includes Extended Experimental Procedures, seven figures, and one table and can be found with this article online at <http://dx.doi.org/10.1016/j.cell.2013.04.023>.

ACKNOWLEDGMENTS

We thank members of the Blenis laboratory for critical discussions and technical assistance. We are also grateful to Li-Huei Tsai (MIT), David Kwiatkowski (BWH), Brendan Manning (HSPH), Wade Harper (HMS), Chi V. Dang (U.Penn), and Takashi Tsukamoto (John Hopkins) for providing critical reagents. We thank Alexandra Grassian and Jonathan Coloff in Joan Brugge's lab (HMS). We thank the Nikon Imaging Center for advice and assistance with microscopy. A.C. is a LAM Foundation Postdoctoral Fellow. S.-M.F. is a German Research Foundation Fellow (FE-1185). G.P. is a Pfizer Fellow of the Life Sciences Research Foundation. S.M.J. was supported in part by a National Research Foundation of Korea Grant funded by the Korean Government. This work was funded by the National Heart, Lung, and Blood Institute grant HL098216 to J.Y., NIH grant AG032375 and Glenn Foundation for Medical Research to M.C.H., and NIH Grant GM51405 to J.B.

Received: June 19, 2012

Revised: March 5, 2013

Accepted: April 10, 2013

Published: May 9, 2013

REFERENCES

Antoniewicz, M.R., Kelleher, J.K., and Stephanopoulos, G. (2007). Accurate assessment of amino acid mass isotopomer distributions for metabolic flux analysis. *Anal. Chem.* **79**, 7554–7559.

Bissler, J.J., McCormack, F.X., Young, L.R., Elwing, J.M., Chuck, G., Leonard, J.M., Schmithorst, V.J., Laor, T., Brody, A.S., Bean, J., et al. (2008). Sirolimus for angiomyolipoma in tuberous sclerosis complex or lymphangioleiomyomatosis. *N. Engl. J. Med.* **358**, 140–151.

Chérasse, Y., Maurin, A.C., Chaveroux, C., Jousse, C., Carraro, V., Parry, L., Deval, C., Chambon, C., Fafournoux, P., and Bruhat, A. (2007). The p300/CBP-associated factor (PCAF) is a cofactor of ATF4 for amino acid-regulated transcription of CHOP. *Nucleic Acids Res.* **35**, 5954–5965.

Choo, A.Y., Kim, S.G., Vander Heiden, M.G., Mahoney, S.J., Vu, H., Yoon, S.O., Cantley, L.C., and Blenis, J. (2010). Glucose addiction of TSC null cells is caused by failed mTORC1-dependent balancing of metabolic demand with supply. *Mol. Cell* **38**, 487–499.

DeBerardinis, R.J., Mancuso, A., Daikhin, E., Nissim, I., Yudkoff, M., Wehri, S., and Thompson, C.B. (2007). Beyond aerobic glycolysis: transformed cells can engage in glutamine metabolism that exceeds the requirement for protein and nucleotide synthesis. *Proc. Natl. Acad. Sci. USA* **104**, 19345–19350.

DeBerardinis, R.J., Lum, J.J., Hatzivassiliou, G., and Thompson, C.B. (2008). The biology of cancer: metabolic reprogramming fuels cell growth and proliferation. *Cell Metab.* **7**, 11–20.

Durán, R.V., Oppliger, W., Robitaille, A.M., Heiserich, L., Skendaj, R., Gottlieb, E., and Hall, M.N. (2012). Glutaminolysis activates Rag-mTORC1 signaling. *Mol. Cell* **47**, 349–358.

Düvel, K., Yecies, J.L., Menon, S., Raman, P., Lipovsky, A.I., Souza, A.L., Triantafellow, E., Ma, Q., Gorski, R., Cleaver, S., et al. (2010). Activation of a metabolic gene regulatory network downstream of mTOR complex 1. *Mol. Cell* **39**, 171–183.

Fendt, S.M., Buescher, J.M., Rudroff, F., Picotti, P., Zamboni, N., and Sauer, U. (2010). Tradeoff between enzyme and metabolite efficiency maintains metabolic homeostasis upon perturbations in enzyme capacity. *Mol. Syst. Biol.* **6**, 356.

Finley, L.W., Carracedo, A., Lee, J., Souza, A., Egia, A., Zhang, J., Teruya-Feldstein, J., Moreira, P.I., Cardoso, S.M., Clish, C.B., et al. (2011). SIRT3 opposes reprogramming of cancer cell metabolism through HIF1 α destabilization. *Cancer Cell* **19**, 416–428.

Frank, C.L., Ge, X., Xie, Z., Zhou, Y., and Tsai, L.H. (2010). Control of activating transcription factor 4 (ATF4) persistence by multisite phosphorylation impacts cell cycle progression and neurogenesis. *J. Biol. Chem.* **285**, 33324–33337.

Gao, P., Tchernyshyov, I., Chang, T.C., Lee, Y.S., Kita, K., Ochi, T., Zeller, K.I., De Marzo, A.M., Van Eyk, J.E., Mendell, J.T., and Dang, C.V. (2009). c-Myc suppression of miR-23a/b enhances mitochondrial glutaminase expression and glutamine metabolism. *Nature* **458**, 762–765.

Gwinn, D.M., Shackelford, D.B., Egan, D.F., Mihaylova, M.M., Mery, A., Vasquez, D.S., Turk, B.E., and Shaw, R.J. (2008). AMPK phosphorylation of raptor mediates a metabolic checkpoint. *Mol. Cell* **30**, 214–226.

Haigis, M.C., and Guarente, L.P. (2006). Mammalian sirtuins—emerging roles in physiology, aging, and calorie restriction. *Genes Dev.* **20**, 2913–2921.

Haigis, M.C., Mostoslavsky, R., Haigis, K.M., Fahie, K., Christodoulou, D.C., Murphy, A.J., Valenzuela, D.M., Yancopoulos, G.D., Karow, M., Blander, G., et al. (2006). SIRT4 inhibits glutamate dehydrogenase and opposes the effects of calorie restriction in pancreatic beta cells. *Cell* **126**, 941–954.

Inoki, K., Li, Y., Zhu, T., Wu, J., and Guan, K.L. (2002). TSC2 is phosphorylated and inhibited by Akt and suppresses mTOR signalling. *Nat. Cell Biol.* **4**, 648–657.

Inoki, K., Zhu, T., and Guan, K.L. (2003). TSC2 mediates cellular energy response to control cell growth and survival. *Cell* **115**, 577–590.

Khan, N., and Mukhtar, H. (2008). Multitargeted therapy of cancer by green tea polyphenols. *Cancer Lett.* **269**, 269–280.

Kim, E., Goraksha-Hicks, P., Li, L., Neufeld, T.P., and Guan, K.L. (2008). Regulation of TORC1 by Rag GTPases in nutrient response. *Nat. Cell Biol.* **10**, 935–945.

Kim, H.S., Patel, K., Muldoon-Jacobs, K., Bisht, K.S., Aykin-Burns, N., Pennington, J.D., van der Meer, R., Nguyen, P., Savage, J., Owens, K.M., et al. (2010). SIRT3 is a mitochondria-localized tumor suppressor required for maintenance of mitochondrial integrity and metabolism during stress. *Cancer Cell* **17**, 41–52.

Kim, S.G., Hoffman, G.R., Poulgiannis, G., Buel, G.R., Jang, Y.J., Lee, K.W., Kim, B.Y., Erikson, R.L., Cantley, L.C., Choo, A.Y., and Blenis, J. (2013). Metabolic stress controls mTORC1 lysosomal localization and dimerization by regulating the TTT-RUVBL1/2 complex. *Mol. Cell* **49**, 172–185.

Le, A., Lane, A.N., Hamaker, M., Bose, S., Gouw, A., Barbi, J., Tsukamoto, T., Rojas, C.J., Slusher, B.S., Zhang, H., et al. (2012). Glucose-independent glutamine metabolism via TCA cycling for proliferation and survival in B cells. *Cell Metab.* **15**, 110–121.

Li, C., Allen, A., Kwagh, J., Doliba, N.M., Qin, W., Najafi, H., Collins, H.W., Matschinsky, F.M., Stanley, C.A., and Smith, T.J. (2006). Green tea polyphenols modulate insulin secretion by inhibiting glutamate dehydrogenase. *J. Biol. Chem.* **281**, 10214–10221.

Lieberman, B.P., Ploessl, K., Wang, L., Qu, W., Zha, Z., Wise, D.R., Chodosh, L.A., Belka, G., Thompson, C.B., and Kung, H.F. (2011). PET imaging of glutaminolysis in tumors by 18F-(2S,4R)4-fluoroglutamine. *J. Nucl. Med.* **52**, 1947–1955.

- Manning, B.D., Tee, A.R., Logsdon, M.N., Blenis, J., and Cantley, L.C. (2002). Identification of the tuberous sclerosis complex-2 tumor suppressor gene product tuberlin as a target of the phosphoinositide 3-kinase/akt pathway. *Mol. Cell* 10, 151–162.
- McCormack, F.X., Inoue, Y., Moss, J., Singer, L.G., Strange, C., Nakata, K., Barker, A.F., Chapman, J.T., Brantly, M.L., Stocks, J.M., et al.; National Institutes of Health Rare Lung Diseases Consortium; MILES Trial Group. (2011). Efficacy and safety of sirolimus in lymphangioleiomyomatosis. *N. Engl. J. Med.* 364, 1595–1606.
- Menon, S., and Manning, B.D. (2008). Common corruption of the mTOR signaling network in human tumors. *Oncogene* 27(Suppl 2), S43–S51.
- Nicklin, P., Bergman, P., Zhang, B., Triantafellow, E., Wang, H., Nyfeler, B., Yang, H., Hild, M., Kung, C., Wilson, C., et al. (2009). Bidirectional transport of amino acids regulates mTOR and autophagy. *Cell* 136, 521–534.
- Possemato, R., Marks, K.M., Shaul, Y.D., Pacold, M.E., Kim, D., Birsoy, K., Sethumadhavan, S., Woo, H.K., Jang, H.G., Jha, A.K., et al. (2011). Functional genomics reveal that the serine synthesis pathway is essential in breast cancer. *Nature* 476, 346–350.
- Qing, G., Li, B., Vu, A., Skuli, N., Walton, Z.E., Liu, X., Mayes, P.A., Wise, D.R., Thompson, C.B., Maris, J.M., et al. (2012). ATF4 regulates MYC-mediated neuroblastoma cell death upon glutamine deprivation. *Cancer Cell* 22, 631–644.
- Reitzer, L.J., Wice, B.M., and Kennell, D. (1979). Evidence that glutamine, not sugar, is the major energy source for cultured HeLa cells. *J. Biol. Chem.* 254, 2669–2676.
- Rouschop, K.M., van den Beucken, T., Dubois, L., Niessen, H., Bussink, J., Savelkoul, K., Keulers, T., Mujcic, H., Landuyt, W., Voncken, J.W., et al. (2010). The unfolded protein response protects human tumor cells during hypoxia through regulation of the autophagy genes MAP1LC3B and ATG5. *J. Clin. Invest.* 120, 127–141.
- Roux, P.P., Ballif, B.A., Anjum, R., Gygi, S.P., and Blenis, J. (2004). Tumor-promoting phorbol esters and activated Ras inactivate the tuberous sclerosis tumor suppressor complex via p90 ribosomal S6 kinase. *Proc. Natl. Acad. Sci. USA* 101, 13489–13494.
- Sancak, Y., Peterson, T.R., Shaul, Y.D., Lindquist, R.A., Thoreen, C.C., Bar-Peled, L., and Sabatini, D.M. (2008). The Rag GTPases bind raptor and mediate amino acid signaling to mTORC1. *Science* 320, 1496–1501.
- Shanware, N.P., Mullen, A.R., DeBerardinis, R.J., and Abraham, R.T. (2011). Glutamine: pleiotropic roles in tumor growth and stress resistance. *J. Mol. Med.* 89, 229–236.
- Vander Heiden, M.G., Cantley, L.C., and Thompson, C.B. (2009). Understanding the Warburg effect: the metabolic requirements of cell proliferation. *Science* 324, 1029–1033.
- Wang, C., Huang, Z., Du, Y., Cheng, Y., Chen, S., and Guo, F. (2010a). ATF4 regulates lipid metabolism and thermogenesis. *Cell Res.* 20, 174–184.
- Wang, J.B., Erickson, J.W., Fujii, R., Ramachandran, S., Gao, P., Dinavahi, R., Wilson, K.F., Ambrosio, A.L., Dias, S.M., Dang, C.V., and Cerione, R.A. (2010b). Targeting mitochondrial glutaminase activity inhibits oncogenic transformation. *Cancer Cell* 18, 207–219.
- West, M.J., Stoneley, M., and Willis, A.E. (1998). Translational induction of the c-myc oncogene via activation of the FRAP/TOR signalling pathway. *Oncogene* 17, 769–780.
- Whitney, M.L., Jefferson, L.S., and Kimball, S.R. (2009). ATF4 is necessary and sufficient for ER stress-induced upregulation of REDD1 expression. *Biochem. Biophys. Res. Commun.* 379, 451–455.
- Wise, D.R., and Thompson, C.B. (2010). Glutamine addiction: a new therapeutic target in cancer. *Trends Biochem. Sci.* 35, 427–433.
- Wise, D.R., DeBerardinis, R.J., Mancuso, A., Sayed, N., Zhang, X.Y., Pfeiffer, H.K., Nissim, I., Daikhin, E., Yudkoff, M., McMahon, S.B., and Thompson, C.B. (2008). Myc regulates a transcriptional program that stimulates mitochondrial glutaminolysis and leads to glutamine addiction. *Proc. Natl. Acad. Sci. USA* 105, 18782–18787.
- Xu, Y., Ho, C.T., Amin, S.G., Han, C., and Chung, F.L. (1992). Inhibition of tobacco-specific nitrosamine-induced lung tumorigenesis in A/J mice by green tea and its major polyphenol as antioxidants. *Cancer Res.* 52, 3875–3879.
- Yamaguchi, S., Ishihara, H., Yamada, T., Tamura, A., Usui, M., Tominaga, R., Munakata, Y., Satake, C., Katagiri, H., Tashiro, F., et al. (2008). ATF4-mediated induction of 4E-BP1 contributes to pancreatic beta cell survival under endoplasmic reticulum stress. *Cell Metab.* 7, 269–276.
- Yang, C., Sudderth, J., Dang, T., Bachoo, R.M., McDonald, J.G., and DeBerardinis, R.J. (2009). Glioblastoma cells require glutamate dehydrogenase to survive impairments of glucose metabolism or Akt signaling. *Cancer Res.* 69, 7986–7993.
- Ye, J., Kumanova, M., Hart, L.S., Sloane, K., Zhang, H., De Panis, D.N., Bobrovnikova-Marjon, E., Diehl, J.A., Ron, D., and Koumenis, C. (2010). The GCN2-ATF4 pathway is critical for tumour cell survival and proliferation in response to nutrient deprivation. *EMBO J.* 29, 2082–2096.
- Yecies, J.L., and Manning, B.D. (2011). mTOR links oncogenic signaling to tumor cell metabolism. *J. Mol. Med.* 89, 221–228.
- Yoshizawa, T., Hinoi, E., Jung, D.Y., Kajimura, D., Ferron, M., Seo, J., Graff, J.M., Kim, J.K., and Karsenty, G. (2009). The transcription factor ATF4 regulates glucose metabolism in mice through its expression in osteoblasts. *J. Clin. Invest.* 119, 2807–2817.
- Young, L.R., Franz, D.N., Nagarkatte, P., Fletcher, C.D., Wikenheiser-Bronk, K.A., Galsky, M.D., Corbridge, T.C., Lam, A.P., Gelfand, M.J., and McCormack, F.X. (2009). Utility of [18F]2-fluoro-2-deoxyglucose-PET in sporadic and tuberous sclerosis-associated lymphangioleiomyomatosis. *Chest* 136, 926–933.
- Zhang, D., Al-Hendy, M., Richard-Davis, G., Montgomery-Rice, V., Sharan, C., Rajaratnam, V., Khurana, A., and Al-Hendy, A. (2010). Green tea extract inhibits proliferation of uterine leiomyoma cells in vitro and in nude mice. *Am. J. Obstet. Gynecol.* 202, 289, e1–e9.
- Zoncu, R., Efeyan, A., and Sabatini, D.M. (2011). mTOR: from growth signal integration to cancer, diabetes and ageing. *Nat. Rev. Mol. Cell Biol.* 12, 21–35.
- Zong, W.X., Ditsworth, D., Bauer, D.E., Wang, Z.Q., and Thompson, C.B. (2004). Alkylating DNA damage stimulates a regulated form of necrotic cell death. *Genes Dev.* 18, 1272–1282.